ELSEVIER

Nuclear Physics A 650 (1999) 283–298

NUCLEAR PHYSICS A

Droplet formation in cold asymmetric nuclear matter

D.P. Menezes [1], C. Providência

Centro de Física Teórica - Depto de Física - Universidade de Coimbra, 3000, Portugal

Received 21 December 1998; revised 8 February 1999; accepted 23 February 1999

Abstract

An extended version of the non-linear Walecka model, with ρ mesons and an electromagnetic field is used to investigate the possibility of phase transitions in cold nuclear matter ($T = 0$), giving rise to droplet formation. Surface properties of asymmetric nuclear matter as the droplet surface energy and its thickness are discussed. The effects of the Coulomb interaction are investigated.

PACS: 21.65.+f; 21.90.+f; 26.60.+c

1. Introduction

The investigation of asymmetric nuclear matter is of particular interest for problems in astrophysics. In fact, neutron-star matter at densities between 0.03 fm^{-3} and nuclear matter density (0.17 fm^{-3}) consists of neutron-rich nuclei immersed in a gas of neutrons [1]. The size of the nuclei is determined by the competition between the surface energy and the Coulomb interaction.

Liquid–gas phase transitions and droplet formation in nuclear reactions as well as the surface properties of nuclear matter have already been extensively discussed in the literature in the context of non-relativistic models, namely within the framework of the Hartree–Fock (HF), Thomas–Fermi (TF) and Extended–Thomas–Fermi approximations (ETF) at finite temperature [2–5] and at zero temperature [6,7]. In particular, in

[1] Permanent address: Depto de Física - CFM - Universidade Federal de Santa Catarina, Florianópolis - SC - CP. 476 - CEP 88.040 - 900, Brazil.

0375-9474/99/$ - see front matter
PII S0375-9474(99)00109-8

Ref. [5] it is shown that the semi-classical TF approximation scheme is reasonably accurate at any temperature.

Within the framework of relativistic models phase transitions in nuclear matter have also been investigated at zero temperature for symmetric semi-infinite nuclear matter [8] and surface properties of asymmetric semi-infinite nuclear matter in Refs. [7,9] and Ref. [10] in terms of a semi-classical treatment. The use of thermodynamical concepts in the study of possible phase transitions in the above problems is done with the underlying assumption that the time required for thermalization and chemical equilibrium is short.

In a previous work, we have investigated droplet formation in a vapour system at finite temperature in the framework of the relativistic Walecka model with non-linear terms (NLWM) [11], which is known to describe adequately the bulk properties of nuclear matter. We have included the Coulomb interaction and worked in the Thomas–Fermi approximation. We have then realized that a more systematic work was necessary in order to estimate the effects of the Coulomb interaction in the production of droplets. For this reason, in the present work we study the conditions for droplet formation and the influence of the electromagnetic field on its production at zero temperature. We determine the conditions for phase coexistence in a multi-component system by building the binodal section [12]. These values determine the initial and boundary conditions which are used in solving numerically the coupled equations of motion obtained in the Thomas–Fermi approximation.

In Section 2 we obtain the equations of motion in the static case and the thermodynamical potential in the framework of the Thomas–Fermi approximation is calculated. In Section 3 the two-phase coexistence is discussed and in Section 4 we present the numerical results and some conclusions are drawn.

2. Extended NLWM and the Thomas–Fermi approximation

In what follows we describe the equation of state of matter within the framework of the relativistic non-linear Walecka model [13,14] with the inclusion of ρ mesons and the electromagnetic field. The self-interaction terms of the scalar meson were shown to be necessary in order to adequately describe nuclear properties [13]. Both the ρ meson and photons are incorporated to account, respectively, for the neutron excess in heavy nuclei and the electromagnetic interaction between the protons [14]. Although we also have in mind the description of neutron star crusts, the pionic degrees of freedom are not considered because their rôle only becomes important for matter much denser than the one investigated in the present work.

In this model the nucleons are coupled to isoscalar–scalar ϕ, isoscalar–vector V^μ, isovector–vector $\boldsymbol{b}^\mu$ meson fields and the electromagnetic field A^μ. The lagrangian density reads

$$\mathcal{L} = \bar{\psi}\left[\gamma_\mu(i\partial^\mu - g_v V^\mu) - \frac{g_\rho}{2}\gamma_\mu \boldsymbol{\tau}\cdot\boldsymbol{b}^\mu - e\gamma_\mu A^\mu\frac{(1+\tau_3)}{2} - (M - g_s\phi)\right]\psi$$

$$+\frac{1}{2}(\partial_\mu\phi\partial^\mu\phi - m_s^2\phi^2) - \frac{1}{3!}\kappa\phi^3 - \frac{1}{4!}\lambda\phi^4 - \frac{1}{4}\Omega_{\mu\nu}\Omega^{\mu\nu} + \frac{1}{2}m_v^2V_\mu V^\mu$$
$$-\frac{1}{4}\boldsymbol{B}_{\mu\nu}\cdot\boldsymbol{B}^{\mu\nu} + \frac{1}{2}m_\rho^2\boldsymbol{b}_\mu\cdot\boldsymbol{b}^\mu - \frac{1}{4}F_{\mu\nu}F^{\mu\nu}, \tag{1}$$

where

$$\Omega_{\mu\nu} = \partial_\mu V_\nu - \partial_\nu V_\mu, \tag{2}$$

$$\boldsymbol{B}_{\mu\nu} = \partial_\mu\boldsymbol{b}_\nu - \partial_\nu\boldsymbol{b}_\mu - g_\rho(\boldsymbol{b}_\mu\times\boldsymbol{b}_\nu), \tag{3}$$

and

$$F_{\mu\nu} = \partial_\mu A_\nu - \partial_\nu A_\mu. \tag{4}$$

The model comprises the following parameter set known as NL1 taken from Ref. [15]: three coupling constants g_s, g_v and g_ρ of the mesons to the nucleons, the nucleon mass $M = 938$ MeV, the masses of the mesons $m_s = 492.25$ MeV, $m_v = 795.36$ MeV, $m_\rho = 763$ MeV, the electromagnetic coupling constant $e = \sqrt{4\pi/137}$, the self-interacting coupling constants $\kappa/M = 2g_s^3\times 2.4578\times 10^{-3}$, $\lambda = -6g_s^4\times 3.4334\times 10^{-3}$, with $C_i^2 = g_i^2M^2/m_i^2$, $i = s,\ v,\ \rho$, given by $C_s^2 = 373.176$, $C_v^2 = 245.458$ and $C_\rho^2 = 149.67$.

From the Euler–Lagrange formalism, we obtain the coupled equations of motion for the scalar, isoscalar–vector, isovector–vector, electromagnetic and nucleon fields, respectively given by

$$(\partial_t^2 - \nabla^2 + m_s^2)\phi = g_s\rho_s - \frac{\kappa}{2}\phi^2 - \frac{\lambda}{6}\phi^3, \tag{5}$$
$$(\partial_t^2 - \nabla^2 + m_v^2)V^\mu = g_v j^\mu \tag{6}$$
$$(\partial_t^2 - \nabla^2 + m_\rho^2)\boldsymbol{b}^\mu = \frac{g_\rho}{2}\boldsymbol{j}^\mu + \frac{g_\rho}{2}(\boldsymbol{b}_\nu\times\boldsymbol{B}^{\nu\mu}) + g_\rho\partial_\nu(\boldsymbol{b}^\nu\times\boldsymbol{b}^\mu), \tag{7}$$
$$(\partial_t^2 - \nabla^2)A^\mu = \frac{e}{2}j^\mu_{\rm em} \tag{8}$$

and

$$i\partial_t\psi = \left[\boldsymbol{\alpha}\cdot\left(-i\boldsymbol{\nabla} - g_v\boldsymbol{V} - \frac{g_\rho}{2}\tau_3\boldsymbol{b} - e\frac{(1+\tau_3)}{2}\boldsymbol{A}\right)\right.$$
$$\left.+\beta(M - g_s\phi) + g_vV^0 + \frac{g_\rho}{2}\tau_3 b^0 + e\frac{(1+\tau_3)}{2}A^0\right]\psi, \tag{9}$$

where the scalar density ρ_s and the baryonic current densities are defined as

$$\rho_s = \langle\bar\psi\psi\rangle,$$
$$j^\mu = \langle\bar\psi\gamma^\mu\psi\rangle,$$
$$\boldsymbol{j}^\mu = \langle\bar\psi\gamma^\mu\boldsymbol{\tau}\psi\rangle,$$
$$j^\mu_{\rm em} = \left\langle\bar\psi\gamma^\mu\left(\frac{1-\tau_3}{2}\right)\psi\right\rangle$$

and $b_3^\mu \equiv (b^0, \boldsymbol{b})$. In the static case there are no currents in the nucleus and the spatial vector components $\boldsymbol{V}$, $\boldsymbol{b}$ and $\boldsymbol{A}$ are zero. Therefore, the equations of motion become

$$\nabla^2\phi = m_s^2\phi + \frac{1}{2}\kappa\phi^2 + \frac{1}{3!}\lambda\phi^3 - g_s\rho_s, \tag{10}$$

$$\nabla^2 V_0 = m_v^2 V_0 - g_v\rho_B, \tag{11}$$

$$\nabla^2 b_0 = m_\rho^2 b_0 - \frac{g_\rho}{2}\rho_3, \tag{12}$$

$$\nabla^2 A_0 = -e\rho_p, \tag{13}$$

where $\rho_B = \rho_p + \rho_n$ and $\rho_3 = \rho_p - \rho_n$ are the baryonic densities, and ρ_p and ρ_n are the proton and neutron densities.

The present work is based on the semi-classical Thomas–Fermi approximation. In this approach the energy of the nuclear system with particles described by the one-body phase-space distribution function $f(\boldsymbol{r}, \boldsymbol{p}, t)$ at position $\boldsymbol{r}$, instant t with momentum $\boldsymbol{p}$ is (only the nuclear matter contribution and interaction terms)

$$E_N = \gamma \mathrm{Tr} \int \frac{\mathrm{d}^3 r \mathrm{d}^3 p}{(2\pi)^3} f(\boldsymbol{r}, \boldsymbol{p}, t)\ h,$$

where

$$h = \begin{pmatrix} \sqrt{(\boldsymbol{p} - \boldsymbol{\mathcal{V}}_p)^2 + (M - g_s\phi)^2} + \mathcal{V}_{p0} & 0 \\ 0 & \sqrt{(\boldsymbol{p} - \boldsymbol{\mathcal{V}}_n)^2 + (M - g_s\phi)^2} + \mathcal{V}_{n0} \end{pmatrix},$$

with

$$\mathcal{V}_{p0} = g_v V_0 + \frac{g_\rho}{2} b_0 + eA_0, \qquad \mathcal{V}_{n0} = g_v V_0 - \frac{g_\rho}{2} b_0,$$

$$\boldsymbol{\mathcal{V}}_p = g_v \boldsymbol{V} + \frac{g_\rho}{2}\boldsymbol{b} + e\boldsymbol{A}, \qquad \boldsymbol{\mathcal{V}}_n = g_v \boldsymbol{V} - \frac{g_\rho}{2}\boldsymbol{b},$$

is the classical effective one-body Hamiltonian and $\gamma = 2$ refers to the spin multiplicity. In the static approximation $\boldsymbol{\mathcal{V}}_p = \boldsymbol{\mathcal{V}}_n = 0$.

The distribution function is given by

$$f = \begin{pmatrix} f_p & 0 \\ 0 & f_n \end{pmatrix},$$

where the distribution functions for protons and neutrons are

$$f_i = \theta(k_{Fi}^2(r) - p^2), \quad i = p, n.$$

The thermodynamic potential is defined as

$$\Omega = E - \sum_{i=p,n} \mu_i B_i, \tag{14}$$

where μ_i is the chemical potential for particles of type i, and B_p, B_n are, respectively, the proton and the neutron number,

$$B_i = \int \mathrm{d}^3 r \rho_i(\boldsymbol{r}, t), \quad i = p, n, \tag{15}$$

with

$$\rho_i = \gamma \int \frac{\mathrm{d}^3 p}{(2\pi)^3} f_i = \frac{\gamma}{6\pi^2} k_{Fi}^3(r).$$

From the above expressions we get for (14)

$$\Omega = \int \mathrm{d}^3 r \left(\frac{1}{2} \left[(\nabla\phi)^2 - (\nabla V_0)^2 - (\nabla b_0)^2 - (\nabla A_0)^2 \right] - V_{ef} \right)$$

with

$$V_{ef} = -\frac{1}{2} \left[m_s^2 \phi^2 + \frac{2}{3!} \kappa \phi^3 + \frac{2}{4!} \lambda \phi^4 - m_v^2 V_0^2 - m_\rho^2 b_0^2 \right]$$
$$-\gamma \int \frac{\mathrm{d}^3 p}{(2\pi)^3} hf + \mu_p \rho_p + \mu_n \rho_n. \tag{16}$$

Minimization of Ω with respect to $k_{Fi}(r)$, $i = p, n$, gives rise to the following conditions:

$$k_{Fp}^2 \left(\mu_p - \sqrt{k_{Fp}^2 + M^{*2}} - g_v V_0 - \frac{g_\rho}{2} b_0 - e A_0 \right) = 0$$

and

$$k_{Fn}^2 \left(\mu_n - \sqrt{k_{Fn}^2 + M^{*2}} - g_v V_0 + \frac{g_\rho}{2} b_0 \right) = 0,$$

where $M^* = M - g_s \phi$ is the effective nucleon mass.

We obtain $k_{Fp} = 0$ and $k_{Fn} = 0$ or, for k_{Fp} or k_{Fn} different from zero,

$$\mu_p = \sqrt{k_{Fp}^2 + M^{*2}} + g_v V_0 + \frac{g_\rho}{2} b_0 + e A_0, \tag{17}$$

$$\mu_n = \sqrt{k_{Fn}^2 + M^{*2}} + g_v V_0 - \frac{g_\rho}{2} b_0. \tag{18}$$

The values of k_{Fp} and k_{Fn} are obtained inverting these last two equations.

The fields that minimize Ω satisfy the equations

$$\frac{\partial V_{ef}}{\partial \phi} = -m_s^2 \phi - \frac{1}{2} \kappa \phi^2 - \frac{1}{3!} \lambda \phi^3 + g_s \rho_s, \tag{19}$$

$$\frac{\partial V_{ef}}{\partial V_0} = m_v^2 V_0 - g_v \rho_B, \tag{20}$$

$$\frac{\partial V_{ef}}{\partial b_0} = m_\rho^2 b_0 - \frac{g_\rho}{2} \rho_3, \tag{21}$$

$$\frac{\partial V_{ef}}{\partial A_0} = -e \rho_p, \tag{22}$$

where

$$\rho_s = \gamma \sum_{i=p,n} \int \frac{\mathrm{d}^3 p}{(2\pi)^3} \frac{M^*}{\epsilon} f_i = \frac{\gamma}{2\pi^2} \sum_{i=p,n} \int_0^{k_{Fi}(r)} p^2 \mathrm{d}p \frac{M^*}{\epsilon}$$

with $\epsilon = \sqrt{p^2 + M^{*2}}$.

Comparing Eqs. (10)–(13) with Eqs. (19)–(22), we see that

$$\nabla^2 \phi = \frac{\mathrm{d}^2 \phi}{\mathrm{d}r^2} + \frac{2}{r} \frac{\mathrm{d}\phi}{\mathrm{d}r} = -\frac{\partial V_{ef}}{\partial \phi}, \tag{23}$$

$$\nabla^2 V_0 = \frac{\mathrm{d}^2 V_0}{\mathrm{d}r^2} + \frac{2}{r} \frac{\mathrm{d}V_0}{\mathrm{d}r} = \frac{\partial V_{ef}}{\partial V_0}, \tag{24}$$

$$\nabla^2 b_0 = \frac{\mathrm{d}^2 b_0}{\mathrm{d}r^2} + \frac{2}{r} \frac{\mathrm{d}b_0}{\mathrm{d}r} = \frac{\partial V_{ef}}{\partial b_0}, \tag{25}$$

$$\nabla^2 A_0 = \frac{\mathrm{d}^2 A_0}{\mathrm{d}r^2} + \frac{2}{r} \frac{\mathrm{d}A_0}{\mathrm{d}r} = \frac{\partial V_{ef}}{\partial A_0}. \tag{26}$$

These coupled differential equations are solved numerically and all relevant quantities (e.g. effective mass, densities, pressure) that depend on the fields are calculated. The discontinuities in the values of $k_{Fp}(r)$ and $k_{Fn}(r)$ discussed above have to be taken into account in the code that solves the differential equations (19–22).

3. Two-phase coexistence

In order to obtain the initial and boundary conditions for the program which integrates the differential equations (23)–(26) we determine the conditions under which two distinct phases can coexist in infinite matter. In this case the electromagnetic field is omitted. In the mean field approximation the meson fields are replaced by their expectation values [16,17],

$$\phi \equiv \langle \phi \rangle = \phi_0, \tag{27}$$

$$V^0 \equiv \langle V^0 \rangle = V_0, \tag{28}$$

$$b^0 \equiv \langle b^0 \rangle = b_0. \tag{29}$$

The substitution of the above expressions in Eqs. (10), (11) and (12) yields

$$\phi_0 = -\frac{\kappa}{2m_s^2}\phi_0^2 - \frac{\lambda}{6}\phi_0^3 + \frac{g_s}{m_s^2}\rho_s, \tag{30}$$

$$V_0 = \frac{g_v}{m_v^2}\rho_B, \tag{31}$$

$$b_0 = \frac{g_\rho}{2m_\rho^2}\rho_3. \tag{32}$$

The thermodynamic quantities of interest are given in terms of the above meson fields. They are the energy density:

$$\mathcal{E} = \frac{\gamma}{2\pi^2}\sum_{i=p,n}\int p^2 dp\sqrt{p^2+M^{*2}}f_i + \frac{m_v^2}{2}V_0^2 + \frac{m_\rho^2}{2}b_0^2 + \frac{m_s^2}{2}\phi_0^2 + \frac{\kappa}{6}\phi_0^3 + \frac{\lambda}{24}\phi_0^4, \tag{33}$$

the pressure

$$P = \frac{\gamma}{6\pi^2}\sum_{i=p,n}\int \frac{p^4 dp}{\sqrt{p^2+M^{*2}}}f_i + \frac{m_v^2}{2}V_0^2 + \frac{m_\rho^2}{2}b_0^2 - \frac{m_s^2}{2}\phi_0^2 - \frac{\kappa}{6}\phi_0^3 - \frac{\lambda}{24}\phi_0^4, \tag{34}$$

and the proton fraction

$$Y_p = \frac{\rho_p}{\rho_B}. \tag{35}$$

We have made use of the geometrical construction [12] to obtain the chemical potentials in the two coexisting phases for each pressure of interest. In a binary system

$$\left(\frac{\partial\mu_p}{\partial Y_p}\right)_P \geqslant 0 \quad \text{and} \quad \left(\frac{\partial\mu_n}{\partial Y_p}\right)_P \leqslant 0, \tag{36}$$

known as diffusive stability, which reflects the fact that in a stable system energy is required to increase the proton concentration while the pressure is kept constant. In order to obtain the binodal section which contains points under the same pressure for different proton fractions, we have used the conditions above and simultaneously solved the following equations:

$$P = P(\nu_p, \nu_n, M^*), \tag{37}$$

$$P = P(\nu_p', \nu_n', M^{*\prime}), \tag{38}$$

$$\mu_i(\nu_p, \nu_n, M^*) = \mu_i(\nu_p', \nu_n', M^{*\prime}), \quad i = p, n \tag{39}$$

$$m_s^2\phi_0 + \frac{\kappa}{2}\phi_0^2 + \frac{\lambda}{6}\phi_0^3 = g_s\rho_s(\nu_p, \nu_n, M^*) \tag{40}$$

and

$$m_s^2\phi_0{}' + \frac{\kappa}{2}\phi_0'^2 + \frac{\lambda}{6}\phi_0'^3 = g_s\rho_s(\nu_p', \nu_n', M^{*\prime}), \tag{41}$$

where $\nu_i = \mu_i - \mathcal{V}_{i0}$, $i = p, n$.

The binodal section is plotted in Fig. 1. For certain values of proton and neutron chemical potentials, the system may be at the same pressure with different densities and proton concentrations, which allows for the possibility of phase transitions. For the sake of completeness, we also show in Table 1 some of the points taken from the binodal section. The results we have chosen as input to the code which solves the differential equations (23)–(26) are displayed in the last three columns of this table.

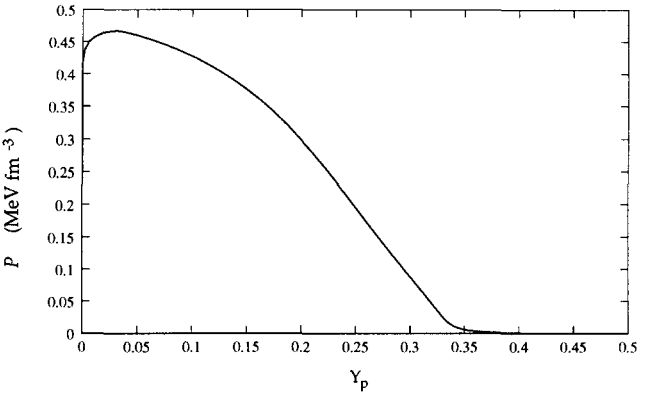

Fig. 1. Binodal section for $T = 0$.

Table 1
Results obtained from the binodal section. The fields are given in units of nucleon mass. In each row the upper (lower) numbers represent the liquid (gas) phase

Y_p	$\mathcal{P}$ (MeV/fm^3)	μ_p (MeV)	μ_n (MeV)	ρ_B (fm^{-3})	$\phi_0 \times 10^{-1}$	$V_{00} \times 10^{-1}$	$b_0 \times 10^{-2}$
0.199	0.308	883.871	949.450	0.095	0.271	0.163	−0.399
0.0				0.050	0.151	0.086	−0.350
0.251	0.193	887.228	946.911	0.105	0.298	0.180	−0.366
0.0				0.043	0.131	0.074	−0.299
0.288	0.110	890.273	944.809	0.113	0.319	0.194	−0.335
0.0				0.036	0.110	0.061	−0.248
0.327	0.020	894.349	942.151	0.122	0.342	0.209	−0.294
0.0				0.022	0.071	0.038	−0.156
0.344	0.0015	896.330	940.954	0.126	0.353	0.217	−0.274
0.0				0.012	0.039	0.020	−0.083
0.373	3×10^{-5}	900.026	938.592	0.134	0.373	0.230	−0.237
0.0				0.0002	0.0008	0.0004	−0.002

4. Numerical results and conclusions

To verify whether the formation of droplets is possible in a finite system, one has to solve numerically the set of coupled equations (23–26). For this purpose, the boundary conditions have to be set within the droplet. We have run a code, written with the help of the Gears stiff integration method, which uses as input the size of the mesh, R_{mesh}, boundary conditions and initial conditions. The size of the mesh determines the size of the droplet. The chemical potentials are output of the program, obtained in accordance with the size of the mesh. In general, the smaller the size of the mesh, the larger the neutron chemical potential. Nevertheless, if we fix the chemical potential according to the values given in Table 1 and do not consider the electromagnetic field, the liquid and gas fields and densities obtained from the binodal section are exactly reproduced respectively at $r = 0$ and at $r > R_{\text{mesh}}$, if the size of the mesh is sufficiently large (at

Table 2
Output results given by the solution of the coupled differential equations without the inclusion of the Coulomb field. Index i refers to $r = 0$.

	$Y_p(i)$	μ_p (MeV)	μ_n (MeV)	σ (MeV fm^{-2})	t (fm)	$R_{\rm mesh}$ (fm)	R_p (fm)	Θ (fm)	$\rho_B(i)$ (fm^{-3})	Y
0	0.215	885.15	949.28	0.051	6.24	11.55	6.81	0.58	0.098	0.378
1	0.251	890.58	946.26	0.093	4.26	7.35	4.41	0.62	0.098	0.341
2	0.292	896.13	943.40	0.154	3.65	5.88	3.63	0.63	0.101	0.320
3	0.333	902.74	940.54	0.226	3.18	4.83	3.03	0.60	0.101	0.303
4	0.364	906.22	938.82	0.307	3.05	4.62	2.97	0.58	0.107	0.307
5	0.429	915.46	934.61	0.564	2.77	4.20	2.82	0.46	0.120	0.333
6	0.462	920.59	931.81	0.781	2.52	4.20	2.89	0.25	0.131	0.400
7	0.497	927.05	927.95	0.998	2.44	4.20	2.95	0.017	0.140	0.493
8	0.500	927.58	927.58	1.004	2.36	4.20	2.95	0.0	0.140	0.5

Table 3
Output results given by the solution of the coupled differential equations with the inclusion of the electromagnetic field. Notice that the last two lines are the results for the same $Y_p(r = 0)$ for different $R_{\rm mesh}$, as discussed in the text

	$Y_p(i)$	μ_p (MeV)	μ_n (MeV)	σ (MeV fm^{-2})	t (fm)	$R_{\rm mesh}$ (fm)	R_p (fm)	Θ (fm)	$\rho_B(i)$ (fm^{-3})	Y
1	0.212	891.06	946.65	0.056	4.94	8.82	5.04	0.54	0.088	0.338
2	0.264	896.58	943.79	0.111	3.65	5.88	3.52	0.62	0.091	0.305
3	0.317	903.10	940.86	0.191	3.19	4.83	2.99	0.60	0.095	0.294
4	0.351	906.58	939.16	0.271	3.05	4.62	2.94	0.58	0.101	0.299
5	0.420	915.84	934.97	0.523	2.77	4.20	2.80	0.46	0.115	0.326
6	0.453	921.00	932.22	0.732	2.52	4.20	2.88	0.26	0.126	0.390
7	0.489	927.52	928.45	0.950	2.44	4.20	2.94	0.01	0.135	0.485
8	0.492	928.06	928.09	0.950	2.36	4.20	2.94	-3×10^{-3}	0.136	0.493
8a	0.491	927.65	927.69	0.990	2.47	4.41	3.12	-4.2×10^{-3}	0.140	0.492

least 12.60 fm for $Y_p = 0.344$, for instance, and larger for smaller proton fractions). However, the aim of this work is to investigate the effects of the Coulomb interaction and we must calculate how the chemical potentials are altered when this interaction is included. Therefore, the chemical potentials must be determined by the program and in Tables 2 and 3 they are given for the smallest size of the mesh, for droplets with at least two protons and a radius of 4.2 fm, for which there is convergence respectively without the inclusion of the Coulomb field and with it, so that we have a coherent comparison method. We must emphasize that the smallest mesh size we have considered was 4.2 fm, which, according to the initial conditions, corresponds to a droplet with at least 14 particles. Using Thomas–Fermi approximation to describe smaller droplets, even though they can exist as solutions of the differential equations, is questionable.

In our code, the boundary conditions are given by

$$\frac{\mathrm{d}\phi}{\mathrm{d}r}(r=0) = \frac{\mathrm{d}V_0}{\mathrm{d}r}(r=0) = \frac{\mathrm{d}b_0}{\mathrm{d}r}(r=0) = \frac{\mathrm{d}A_0}{\mathrm{d}r}(r=0) = 0$$

and for $r = R_{\rm mesh}$,

$$\frac{{\rm d}\phi}{{\rm d}r} + \left(m_s + \frac{1}{R_{\rm mesh}}\right)\phi = \left(m_s + \frac{1}{R_{\rm mesh}}\right)\phi_g,$$

where ϕ_g is the value we expect for the gas field, obtained from the binodal section (given also in Table 1), and similar equations for V_0 and b_0. For A_0 we have

$$\frac{{\rm d}A_0}{{\rm d}r} + \frac{A_0}{R_{\rm mesh}} = 0,$$

or, considering the electron screening, A_0 is zero at the last point of the mesh,

$$A_0(R_{\rm mesh}) = 0.$$

Both boundary conditions give similar results for the physical properties we have calculated.

As initial guesses for the meson fields we have used Fermi like functions. The values for $r = 0$ were obtained from the binodal section. An initial guess for the electromagnetic field is the field of a homogeneous spherical distribution of protons. We suppose that the droplets are formed in an electrically neutral environment, as we find in neutron stars. We assume that the droplet is small enough for the electrons to spill out from it almost completely, e.g. the electrons accumulate around the droplets giving rise to a shielding effect. We have checked that the surface properties of the droplets do not depend on the radius of the electron distribution.

The radius $R_{\rm mesh}$ fixes the neutron and proton chemical potentials and, therefore, the number of neutrons and protons. We have considered that convergence has been achieved when the fields and the baryonic density do not vary more than 10^{-3} per cent from one run to the following one.

Some quantities of interest to study the surface properties are the two *squared-off* radii R_n and R_p in the spherical geometry, defined as

$$\int_0^{R'} \rho_n(r) r^2 {\rm d}r = \frac{1}{3}\left[\rho_{n,i} R_n^3 + \rho_{n,f}(R'^3 - R_n^3)\right], \tag{42}$$

and

$$\int_0^{R'} \rho_p(r) r^2 {\rm d}r = \frac{1}{3}\left[\rho_{p,i} R_p^3 + \rho_{p,f}(R'^3 - R_p^3)\right], \tag{43}$$

where ρ_i refers to the liquid density, ρ_f to the gas density, R' is larger than the size of the mesh and corresponds to the value of r where $|f(r) - f_g| < 10^{-8}$ with f being either a meson field or the baryonic density at r and f_g the corresponding gas value. Another important quantity is the thickness of the region at the surface with extra neutrons known as *neutron skin*. The *neutron skin thickness* is given by [10]

$$\Theta = R_n - R_p. \tag{44}$$

These quantities are computed for the droplet solutions we obtain and given in Tables 2 and 3 without and with the Coulomb interaction respectively.

The droplet surface energy and thickness are obtained from the energy of a system with a fixed number of particles $B = B_p + B_n$, in which a droplet of arbitrary size grows in the background of the vapour phase. The energy reads

$$E = \int 4\pi r^2 \mathrm{d}r \left[\frac{1}{2}\left(\left(\frac{\mathrm{d}\phi}{\mathrm{d}r}\right)^2 - \left(\frac{\mathrm{d}V_0}{\mathrm{d}r}\right)^2 - \left(\frac{\mathrm{d}b_0}{\mathrm{d}r}\right)^2 - \left(\frac{\mathrm{d}A_0}{\mathrm{d}r}\right)^2\right) - V_{ef}\right] + \mu_p B_p + \mu_n B_n, \tag{45}$$

where V_{ef} is given in Eq. (16). If the Coulomb field is neglected, E can be rewritten in the small surface thickness approximation as [18]

$$E = \int 4\pi r^2 \mathrm{d}r \left[\left(\frac{\mathrm{d}\phi}{\mathrm{d}r}\right)^2 - \left(\frac{\mathrm{d}V_0}{\mathrm{d}r}\right)^2 - \left(\frac{\mathrm{d}b_0}{\mathrm{d}r}\right)^2 - C\right] + \mu_p B_p + \mu_n B_n, \tag{46}$$

where C is a constant. For droplets with radius R and volume V,

$$E(R) = 4\pi R^2 \sigma - CV + \mu_p B_p + \mu_n B_n. \tag{47}$$

The surface energy per unit area of these droplets in the small surface thickness approximation is then

$$\sigma = \int_0^\infty \mathrm{d}r \left[\left(\frac{\mathrm{d}\phi}{\mathrm{d}r}\right)^2 - \left(\frac{\mathrm{d}V_0}{\mathrm{d}r}\right)^2 - \left(\frac{\mathrm{d}b_0}{\mathrm{d}r}\right)^2\right]. \tag{48}$$

When the Coulomb field is included, the small surface thickness approximation is not valid. However, as the electromagnetic interaction should not contribute to surface properties directly, we have considered the same definition for the surface energy and defined the Coulomb energy as

$$E_c = \int 4\pi r^2 \mathrm{d}r \left[-\frac{1}{2}\left(\frac{\mathrm{d}A_0}{\mathrm{d}r}\right)^2 + e\rho_p A_0\right]. \tag{49}$$

In order to check the validity of Eq. (48) for symmetric and almost symmetric matter, we have also parametrized the total energy of the droplet, excluding the Coulomb energy given in Eq. (49), in terms of the volume and surface energies as

$$E = -aA + b4\pi (r_0)^2 A^{2/3}, \tag{50}$$

where $A = B_p + N$, with $N = B_n - B_g$ and B_g is the number of neutrons in the gas, $r_0 = RA^{-1/3}$ and R is the radius of the droplet given by

$$R^3 = \frac{R_n^3(\rho_{n,i} - \rho_{n,f}) + R_p^3(\rho_{p,i} - \rho_{p,f})}{(\rho_{n,i} - \rho_{n,f} + \rho_{p,i} - \rho_{p,f})}.$$

The bulk contribution for the binding energy is given by $-a$ and the surface energy by b. For $Y_p(i) = 0.497$ (Table 2, without the Coulomb field) we have obtained $r_0 = 1.12$ fm, $a = 16.45$ MeV, and $b = 1.20$ MeV/fm^2. The same procedure was followed for $Y_p(i) = 0.489$ (Table 3, with the Coulomb field) and the parameters are $a = 16.14$ MeV, and $b = 1.18$ MeV/fm^2 for $r_0 = 1.16$ fm. In both cases, the numbers obtained from the parametrization are very close to the ones found by our code, which leads us to the conclusion that the definition for the surface energy given in Eq. (48), albeit approximate, is a good one.

The surface thickness t is defined as the width of the region where the density drops from $0.9\rho_{B0}$ to $0.1\rho_{B0}$, where ρ_{B0} is the baryonic density at $r = 0$, after subtracting the background gas density. According to Ref. [13], for $T = 0$, σ should be of the order of 1.25 MeV fm^{-2} and t of the order of 2.2 fm. These values are related with saturation properties within the droplet. We obtain larger droplets than the ones shown in Tables 2 and 3 if larger sizes of the mesh are considered. The surface energy increases with the size of the droplet until a saturation value is reached. For symmetric matter with the Coulomb field switched off, we have obtained for the saturation value of the surface energy $\sigma = 1.22$ MeV/fm^2 for a droplet with radius 7.35 fm or larger. With the inclusion of the Coulomb field, we have obtained $\sigma = 1.21$ MeV/fm^2 for a droplet with radius 8.40 fm or larger. If we keep increasing the mesh, the above values do not vary more than one per cent.

At this point some comments are in order. We have chosen to compare data corresponding to the same value of the boundary conditions for a fixed size of the mesh. For initial proton fractions smaller than 0.2 we do not get droplet solutions (with Coulomb field included or not). For $Y_p(i) = 0.21$ the surface energy is already very small, 0.05 MeV/fm^2 (see Tables 2 and 3). Smaller initial proton fraction implies even smaller surface energy. In principle we obtain a solution as far as σ is still positive. For $Y_p(i) = 0.2$ we get a solution with $\sigma = 0.033$ MeV/fm^2. Before drawing our conclusions, we would like to emphasize that in our calculations, the proton and neutron numbers are never fixed. They are output of the results obtained for the fields and densities, which are solutions of the differential equations.

In Tables 2 and 3 we display the results found for the proton fractions at $r = 0$ ($Y_p(i)$), the chemical potentials, the surface energy, its thickness, the smallest size of the mesh for which convergence is achieved, R_p, the neutron skin thickness, the central density and the *proton fraction within the droplet* defined as

$$Y = \frac{B_p}{B_p + N}.$$

The boundary conditions in entry i, $i = 1, \ldots, 8$ of both tables are the same. Notice that there is a small discrepancy between the proton and neutron chemical potentials given in Table 1 and the ones displayed in Tables 2 and 3 for the reasons explained in the beginning of this section. The difference between the values for μ_p and μ_n in Tables 2 and 3 are due to the inclusion of the Coulomb interaction.

In the cases we have considered, the vapour phase has a zero proton fraction but a

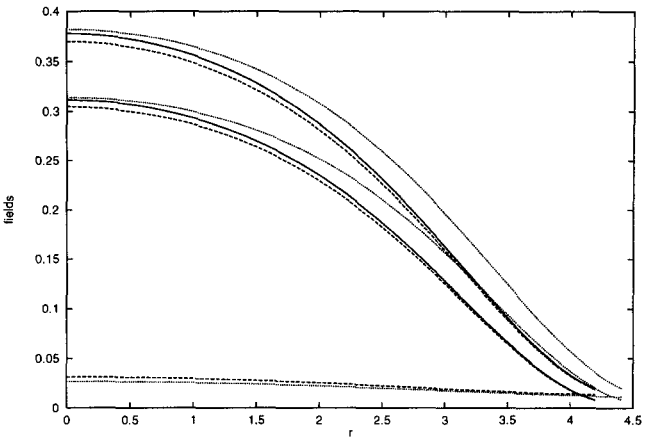

Fig. 2. $g_s\phi$, $g_v V_0$ and $eA_0 \times 10$ (in this order, from top to bottom) are shown in terms of r. The fields are given in nucleon mass units and are obtained for symmetric nuclear matter. The solid lines are the results obtained without the Coulomb interaction and $R_{\text{mesh}} = 4.2$ fm. The dashed lines are the results obtained with the Coulomb interaction for $R_{\text{mesh}} = 4.2$ fm and the dotted lines for $R_{\text{mesh}} = 4.4$ fm. The Coulomb field is plotted in a different scale! (see last two lines of Table 3).

non-zero neutron density except for symmetric nuclear matter, when the gas density is zero. This fact is interpreted as a droplet with a given proton concentration (the phase of higher density) in equilibrium with a gas of drip neutrons. We have also verified that the larger the proton fraction, the smaller the size of the mesh for which convergence is first achieved. This may be due to the decrease of neutron–proton asymmetry and therefore, the increase of the droplet binding.

From Tables 2 and 3, one can check that the surface energy σ increases with the initial proton fraction and its thickness t decreases. In fact, the larger the proton fraction the less important is the contribution from the b_0 field in the σ calculation as can be seen from (48).

In the same tables the squared-off proton radius and the neutron skin thickness are also shown. The proton radius decreases with the increase of the proton fraction at $r = 0$ for a fixed size of the mesh. This behaviour could be a consequence of the increase of the droplet binding. In order to understand better the behaviour of the neutron skin thickness Θ, we have included in Tables 2 and 3 the proton fraction within the droplet, Y. One can observe that Θ decreases with the increase of Y for a fixed size of the mesh, so that droplets with a smaller percentage of protons inside present thicker neutron skins.

The best way to understand the behaviour of the fields and baryonic densities is by plotting them. As an example, in Fig. 2 we plot the fields which are solutions of the coupled equations for symmetric nuclear matter, given in the last line of Table 2 and last two lines of Table 3. The curves show the results obtained without and with the Coulomb interaction for two distinct cases. In the first case, the calculation with and without the Coulomb was done for the same mesh size, e.g. 4.2 fm. This is the standard procedure adopted for all other proton fractions, except when the code with the Coulomb interaction does not converge and a larger size of the mesh has to be used. In the second

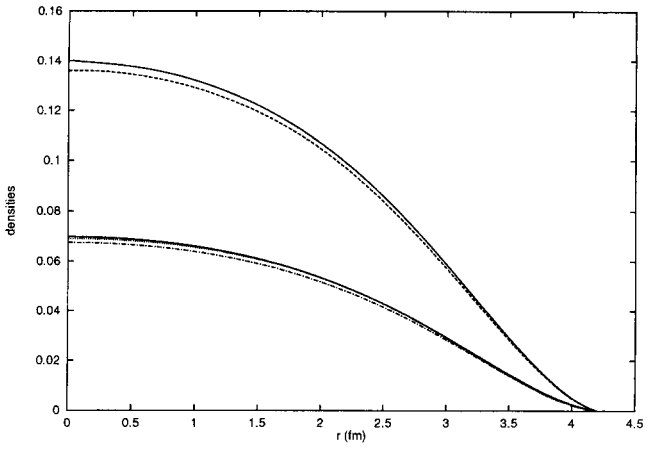

Fig. 3. The density profiles for the baryons $\rho_B(r)$ (top two curves, with - dashed line - and with no Coulomb field - full line), the neutrons $\rho_n(r)$ and the protons $\rho_p(r)$ (last three curves) in fm^{-3} are plotted for symmetric nuclear matter. The solid curves are the densities obtained without the inclusion of the electromagnetic field. Notice that, in this case, ρ_p and ρ_n coincide. The dot-dashed line and the dotted line represent respectively ρ_p and ρ_n with the Coulomb interaction. The size of the mesh is 4.2 fm in both calculations.

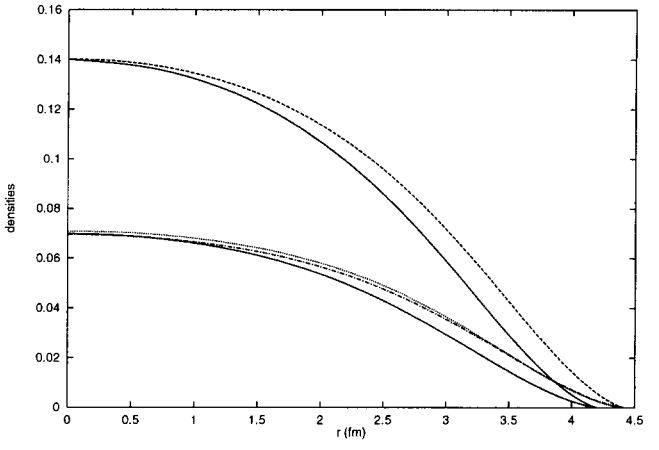

Fig. 4. The same as in Fig. 3, but the Coulomb interaction is taken into account in a different manner, since the size of the mesh in both calculations is slightly different (please, refer to Table 3).

case, we have increased slightly the size of the mesh so that the baryonic density at $r = 0$ coincides in both cases. The results are displayed in the last line of Table 3. This procedure allows for the interpretation of the effect of the Coulomb field in a system with the same central density, as will be discussed below. The baryonic density plotted in Fig. 3 for the first case mentioned above and Fig. 4 for the second one represents a droplet of the liquid phase (small r) in the background of the vapour phase (large r).

In Fig. 5 we plot the fields for asymmetric nuclear matter corresponding the entry 3 in Tables 2 and 3 ($Y_p \sim 0.3$) and in Fig. 6 the corresponding density profiles.

Figs. 3 and 6 show the behaviour of the total baryonic density. One can see that it

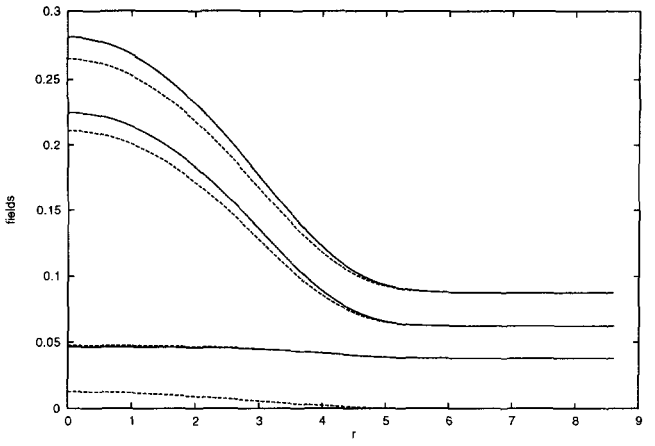

Fig. 5. $g_s\phi$, $g_v V_0$, $g_\rho b_0 \times (-2)$ and $eA_0 \times 10$ (in this order, from top to bottom) are shown in terms of r. The fields are given in nucleon mass units and correspond to entry 3 in Tables 2 and 3 ($Y_p \sim 0.3$). The solid lines are the results obtained without the Coulomb interaction. The dashed lines are the results obtained with the Coulomb interaction for the same size of the mesh as the previous result.

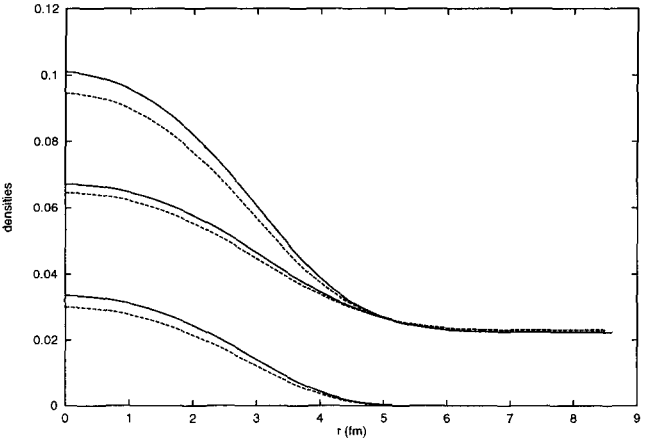

Fig. 6. From top to bottom the density profiles for the baryons $\rho_B(r)$, the neutrons $\rho_n(r)$ and the protons $\rho_p(r)$ in fm^{-3} are plotted for $Y_p \sim 0.3$. The solid and dashed lines correspond respectively to the results without and with the Coulomb field. In this case, ρ_p and ρ_n do not coincide.

falls from the initial liquid density to the vapour density, which is zero for symmetric nuclear matter and different from zero in the other cases.

Concerning the importance of the Coulomb interaction and its consequences in the droplet formation, one can see, from Figs. 3 and 6, that the proton and neutron densities are indeed modified by the electromagnetic field, as pointed out in [2]. For the same value of Y_p at $r = 0$ and the same size of the mesh, an effect of the electromagnetic field, in the present calculation, is to decrease the number of particles in the droplet, since the central density becomes smaller. The protons and neutrons are pushed to the surface, which is confirmed in Fig. 4. The size of the droplet with the Coulomb field switched

on has to be increased with respect to the size of the droplet with no Coulomb field, in order to have the same baryonic density at $r = 0$. Comparing the last two columns of Tables 2 and 3 it is seen that the Coulomb field decreases the central density and the fraction of protons in the droplet, for the same boundary conditions, e.g. the same meson fields in the vapour phase. Another effect already referred to is the fact that droplets with a central $Y_p < 0.2$ are not stable. From Tables 2 and 3 we also conclude that surface properties such as σ, t and Θ are not modified or only slightly modified by the presence of the electromagnetic field. In summary, the Coulomb field affects mainly the bulk properties of the droplets, reducing the binding energy and obliging the particles to be further apart.

Acknowledgements

We would like to thank Dr. Hans Walliser for giving us his FORTRAN code which solves the differential equations and for his useful suggestions. One of the authors (DPM) would like to acknowledge the warm hospitality of the Centro de Física Teórica of the University of Coimbra, where this work was accomplished. This work has been partially supported by Capes, Brazil, and JNICT, Portugal, under the contracts PRAXIS/PCEX/C/13/96, CERN/S/FIS/1034/95 and PRAXIS/2/2.1/FIS/451/94.

References

[1] S.L. Shapiro and S.A. Teukolsky, Black Holes, White Dwarfs and Neutron Stars, (Wiley, New York, 1983);
C.J. Pethick, D.G. Ravenhall and C.P. Lorenz, Nucl. Phys. A 584 (1995) 675.
[2] P. Bonche, S. Levit and D. Vautherin, Nucl. Phys. A427 (1984) 278; Nucl. Phys. A436 (1985) 265.
[3] D.G. Ravenhall, C.J. Pethick and J.M. Lattimer, Nucl. Phys. A407 (1983) 571; G. Baym, H.A. Bethe and C.J. Pethick, Nucl. Phys. A 175 (1971) 225; D.G. Ravenhall, C.D. Bennet and C.J. Pethick, Phys. Rev. Lett. 28 (1972) 978.
[4] A.L. Goodman, J.I. Kapusta and A.Z. Mekjian, Phys. Rev. C 30 (1984) 851.
[5] E. Suraud, Nucl. Phys. A 462 (1987) 109.
[6] K. Kolehmainen, M. Prakash, J.M. Lattimer and J.R. Treiner, Nucl. Phys. A 439 (1985) 535.
[7] W.D. Myers, W.J. Swiatecki and C.S. Wang, Nucl. Phys. A 436 (1985) 185.
[8] F.J.B. Salzedas, MSc. Dissertation, Universidade de Coimbra (1995).
[9] D. Von Eiff, J.M. Pearson, W. Stocker and M.K. Weigel, Phys. Lett. B 324 (1994) 279.
[10] M. Centelles, M. Del Estal and X. Viñas, preprint, 1997.
[11] D.P. Menezes, C. Providência, electronic archive nucl-th/9809078 - submitted to publication.
[12] M. Barranco and J.R. Buchler, Phys. Rev. C 22 (1980) 1729.
[13] J. Boguta and A.R. Bodmer, Nucl. Phys. A292 (1977) 413; A.R. Bodmer and C.E. Price, Nucl. Phys. A505 (1989) 123; A.R. Bodmer, Nucl. Phys. A526 (1991) 703.
[14] Y.K. Gambir, P. Ring and A. Thimet, Ann. Phys. 198 (1990) 132; H. Berghammer, D. Vretenar and P. Ring, Phys. Lett. B 296 (1992) 290; H. Berghammer, D. Vretenar and P. Ring, Nucl. Phys. A 560 (1993) 1014.
[15] C. Speicher, E. Engel and R.M. Dreizler, Nucl. Phys. A562 (1993) 569.
[16] H. Müller and B.D. Serot, Phys. Rev. C 52 (1995) 2072.
[17] Sumiyoshi and Toki, Astroph. J. 422 (1944) 700.
[18] M. Nielsen, J. Providência, J. Phys. G 16 (1990) 649.